Nature and origin of an undetected seismic phase in waveforms from Southern Tyrrhenian (Italy) intermediate-depth and deep earthquakes: first evidence for the phase-A in the subducted uppermost lithospheric mantle?

Published version:

DOI:10.1016/j.tecto.2023.229919

Nature and Origin of an Undetected Seismic Phase in Waveforms from Southern Tyrrhenian (Italy) Intermediate-Depth and Deep Earthquakes: first evidence for the Phase-A in the Subducted Uppermost Lithospheric Mantle?

T. Ninivaggi[1], G. Selvaggi[1], S. Mazza[1], M. Filippucci[2], F. Tursi[3], & W. Czuba[4]

[1] Istituto Nazionale di Geofisica e Vulcanologia, Rome, Italy.

[2] Università degli Studi di Bari "Aldo Moro", Dipartimento di Scienze della Terra e Geo-ambientali, Bari, Italy.

[3] Università degli studi di Padova, Dipartimento di Geoscienze, Padua, Italy.

[4] Institute of Geophysics, Polish Academy of Sciences, Warsaw, Poland.

Corresponding author:

Teresa Ninivaggi

E-mail Address: teresaninivaggi@gmail.com

Postal Address: Via E. De Amicis, 12 – Altamura (Bari) 70022

Abstract

We have found a previously unreported seismic phase in seismograms of European seismic stations from intermediate-depth and deep earthquakes of the Southern Tyrrhenian subduction zone. We observe this phase at stations from 6 to 9 degrees from the epicentre, towards north. Only seismograms of earthquakes located in a well-defined region of the slab, in the depth range of 215–320 km, show this secondary phase. In this work, we describe the nature and possible origin of this phase and we provide a simple 2D model to explain the observed arrival times. Our analyses reveal that this secondary phase propagates downward in a narrow, high velocity layer, possibly

located within the deepest part of the slab. We suggest that this layer reveals the presence of the dense hydrous magnesium silicate *phase A*, introduced from petrological laboratory experiments, inferred to carry water in the upper mantle and predicted to be found in cold subduction zones.

Key Words:

Later seismic arrival/phase

Waveforms analyses

Intermediate and deep seismicity

Southern Tyrrhenian Subduction Zone

Mineral phase A

1 Introduction

Seismograms of deep earthquakes from many subduction zones show later phases. Most of these observations come from the Pacific subduction zones and they have been widely used to get useful indication on the geometric characteristics of subducting slabs (Hasegawa et al., 1978; Matsuzawa et al., 1986; Ohmi & Hori, 2000; Zhao et al., 1997). These phases, beside the depth phases, are generally associated to *P (S)* waves converted or reflected at the upper slab interface from the direct *S (P)* waves (Ohmi & Hori, 2000; Zhao, 2019; Zhao et al., 1997, Fukao et al., 1978; Obara & Sato, 1988). Observations of dispersive and complicated wave trains are also relevant in seismograms of deep earthquakes as they provide important implications for the petrological properties of subducted lithosphere. For example, dispersive high frequency trains of *P*- and *S*-waves observed at the fore-arc seismic stations of the Hellenic Trench from intermediate depth earthquakes reveal the presence of a low velocity channel in the upper part of the slab (Abers, 2000, 2005; Essen et al., 2009; Hori, 1990; Martin et al., 2003; Martin & Rietbrock, 2006). The low velocity channel is an important finding to trace water path within the subduction process. Similar characteristics were also found in seismograms of Calabria stations, recorded from deep earthquakes of the Southern Tyrrhenian subduction zone and interpreted as generated by small scale heterogeneities within the slab (Sun et al., 2014).

Working on seismograms of a deep earthquake from the Southern Tyrrhenian subduction zone occurred in 2011, we noticed a clear secondary phase, few seconds after the direct *P*-wave, at stations located some hundreds of km away from the epicenter towards north (Figure 1).

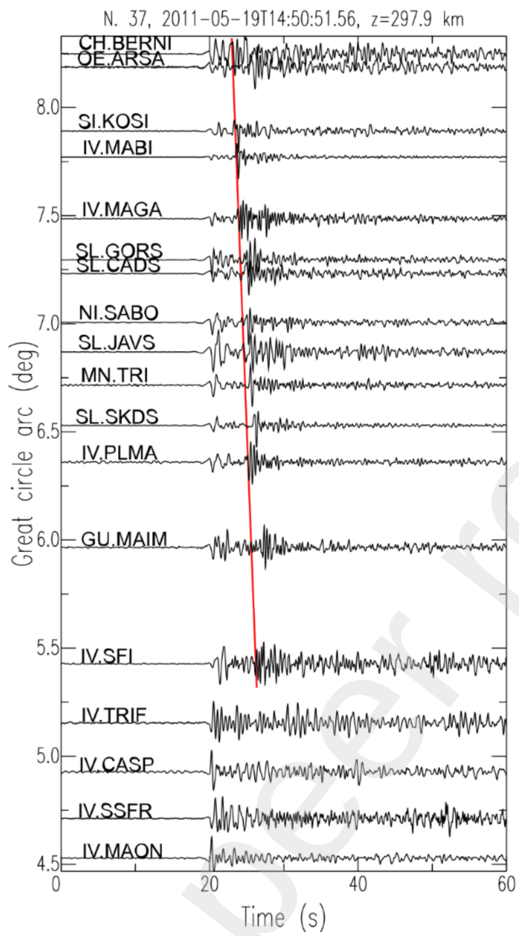

Figure 1. *Time-distance vertical seismograms of the 2011 event aligned with P arrival time at 20 s. The red line marks the secondary phase arrivals.*

This phase, that we have called *x-phase*, disappears at stations located in Central and northern Europe (Figure 2). In a first stage of the work, we accepted the same lines of interpretation of the quoted literature, but we soon understood that the arrival times of the phase we were looking at were not consistent neither with a sP (pS) converted phase, nor with a guided wave. This because the lag times after direct arrivals are constant or increase with distances for converted or guided waves, respectively (Hori, 1990; Zhao et al., 1997). The difference in arrival times between our phase and the direct *P*-wave decreases with the epicentral distance and it does it in a way that excludes such interpretations.

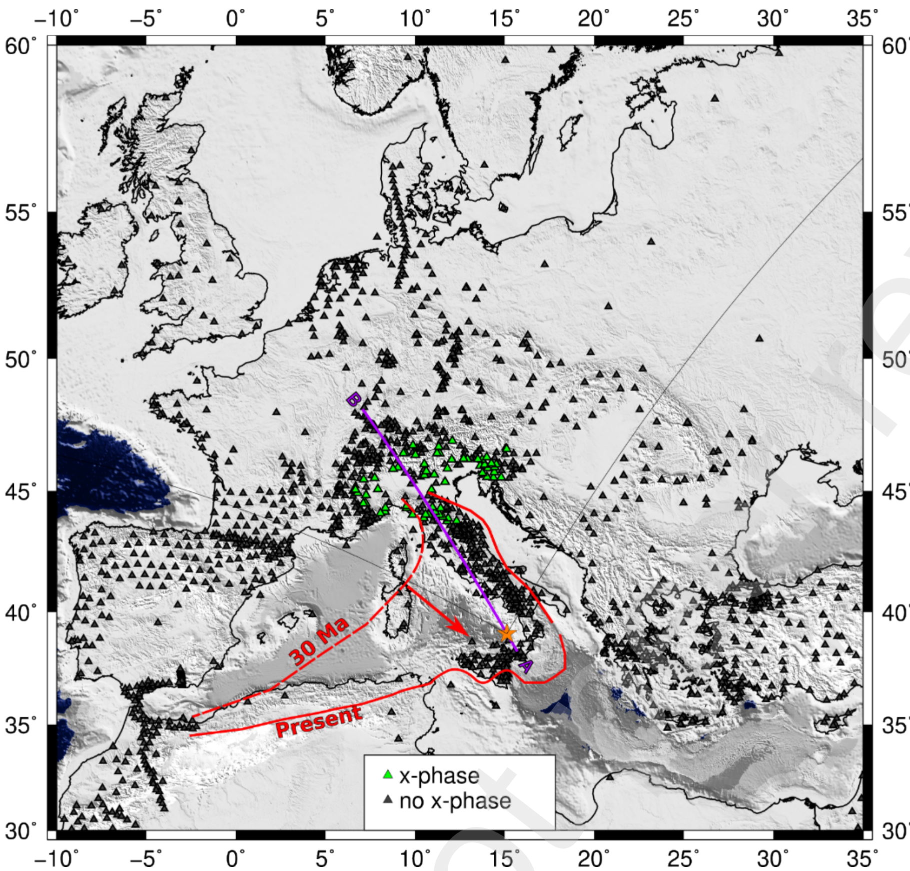

Figure 2 *– Stations which recorded the x-phase (green triangles). Seismograms of stations in black do not show the later arrival. Section trace AB of the Figure 9, passing from the 2011 earthquake (n. 37). The red lines delineate the old (30 Ma) and the present subduction signature. The two thin black lines delineate the azimuths 300° and 30° clockwise with respect to the epicentre.*

We decided, then, to investigate a wider dataset composed of the 43 deep and largest earthquakes of the Southern Tyrrhenian subduction zone and to perform classical waveforms analyses to derive the main seismological features of the unreported phase. We, finally, made a 2D ray path modelling to infer the origin of the *x-phase*. In this paper, we first describe the dataset and the observations related to the seismic phase then we use the results to constrain a 2D model of the slab to explain the observations. One major point we discuss in this work is the possible identification in the subducting slab of a dense magnesium silicate mineral phase carrying water in the upper mantle and the petrological implication of this finding.

2. Tectonic setting

The Southern Tyrrhenian basin is the result of the Ionian lithosphere rollback and associated opening of the back arc basin that lasted for 80 Myr (Faccenna et al., 2001). Based on tomographic images, plate tectonics reconstructions and geological data, Faccenna et al., (2001) recognized multiple evolutionary stages of the subduction process characterized by different back-arc opening rates, sometimes as fast as 30-40 mm/yr (Figure 2). The slab should have reached the 660 km transition zone after about 60-70 Myr of subduction process (Faccenna et al., 2001). GNSS velocity field (D'Agostino et al., 2011) shows that the present day roll back, if any, of the Ionian lithosphere could be at the level of 1 mm/yr, much slower than in the past. The subduction of the Ionian lithosphere beneath the Calabrian arc and the Tyrrhenian Sea is nowadays marked by an intense intermediate and deep seismicity. The occurrence of deep earthquakes beneath the Southern Tyrrhenian Sea is well known since the seventies, and reported in a wide literature (Ritsema, 1972; see also Chiarabba et al., 2008; Scarfì et al., 2018; Selvaggi & Chiarabba, 1995). The seismicity distribution clearly defines a NW-dipping Wadati-Benioff plane from the Ionian Sea towards the central Tyrrhenian Sea. Earthquakes can be as deep as 600 km (Figure 3). Seismicity distribution and tomographic images show that the descending Ionian slab is very steep

(~70°) in the first 300-350 km and starts flattening below those depths (Chiarabba et al., 2008; Cimini & Marchetti, 2006; Lucente et al., 1999; Scarfì et al., 2018; Spakman et al, 1993).

The slab is seismically continuous only in its southwestern part, beneath the Aeolian Islands (Figure 3b) while, in the north-eastern portion, along the Calabrian coasts, the slab is mostly aseismic between 100 km and 250 km depth (Figure 3c). The aseismic part of the slab has been interpreted as an indication that the slab is dying out along a horizontal break-off that propagates in a scissor-type mode (Amato et al., 1993; Scarfì et al., 2018; Spakman et al., 1993).

The Southern Tyrrhenian slab is in down dip shortening in a large part of it, from about 100 km down to 400 km depth, and the magnitude of earthquakes increases with depth (Frepoli et al., 1996; Selvaggi, 2001). The largest earthquake occurred in 1938 and had a magnitude of 7.1 (Anderson & Jackson, 1987). The depth estimate was 290 km and it is one of the largest earthquake ever recorded in Italy. The way the slab deforms suggests that the gravitational pull is probably the main driving force of the subduction.

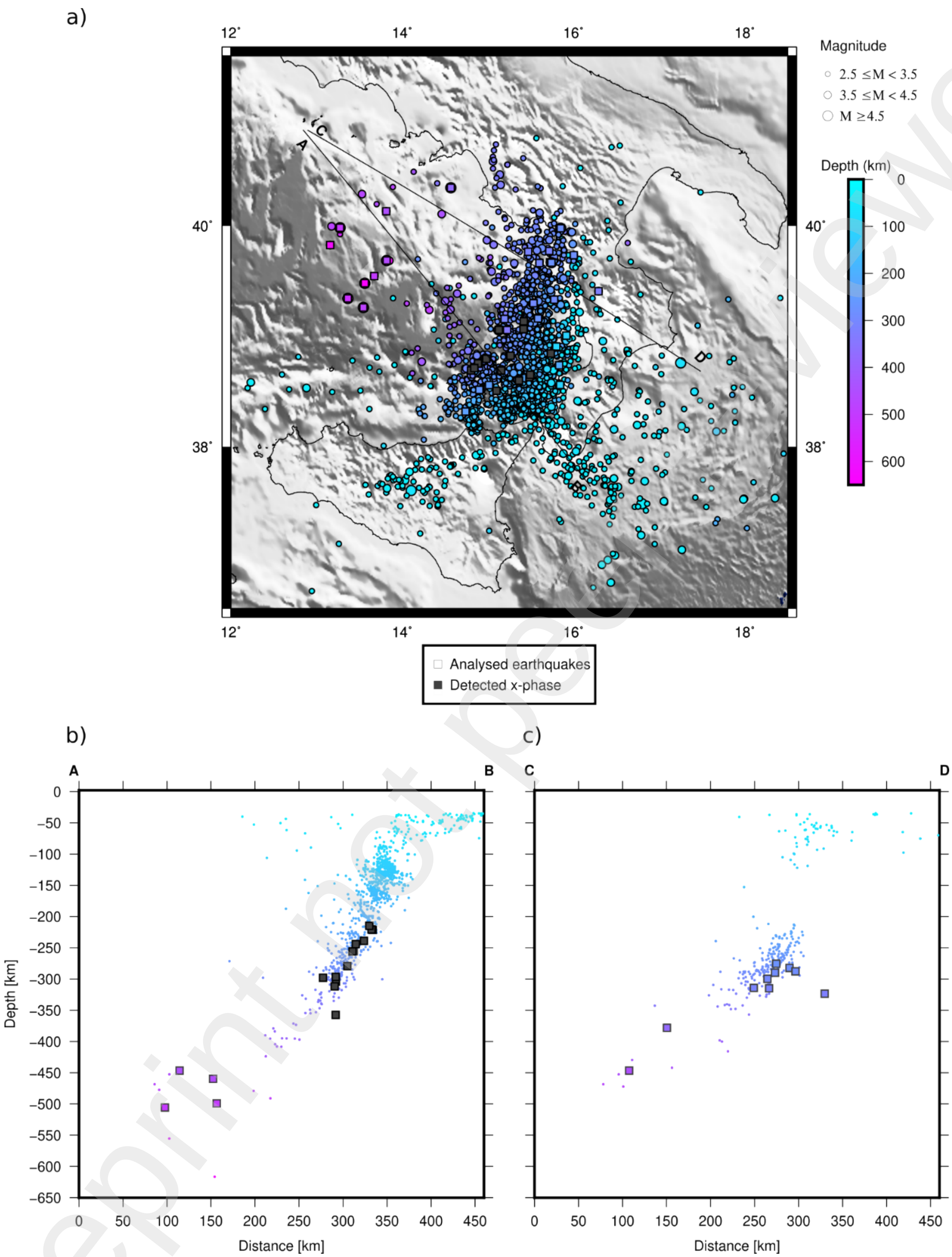

Figure 3 - *Seismicity map of the Southern Tyrrhenian Subduction Zone from 1990 to 2020.* ***(a)*** *Squares are the 43 analysed earthquakes; grey filled squares are those earthquakes where we*

recognised the x-phase. ***(b)*** *Vertical cross-sections perpendicular to the strike of the southwestern part of the slab (AB) and* ***(c)*** *its north-eastern part (CD).*

3. Data and Methods

We decided to make a systematic analysis of deep earthquakes from the Tyrrhenian subduction zone to further investigate and constrain the previous observations on the *x-phase*. We selected the 43 largest earthquakes from 1990 to 2020 (ML ≥ 4.5) located in Southern Tyrrhenian region from the INGV Italian Seismological Instrumental and Parametric Database (http://cnt.rm.ingv.it/iside). The depth range is between 100 km and 644 km. The earthquakes list and additional examples of the computed analysis from the whole dataset are available in the supplementary material.

We extracted the digital waveforms of the earthquakes from the European Integrated Data Archive (EIDA, http://eida.ingv.it/) and from Incorporated Research Institutions for Seismology Data Management Centre (IRIS DMC, https://ds.iris.edu/ds/nodes/dmc/data/types/waveform-data/). The selected seismic stations are from 10° up to 71° North in latitude (from Central Africa to north Norway) and between 10° West and 50° East in longitude (from Portugal to eastern Turkey). We used seismograms from broadband high gain seismometers (HH or BH streams) for each earthquake, when available. If they were not, we used short period high gain seismometers (EH or SH), especially for the oldest earthquakes. To analyse the whole dataset, i.e. more than 25,000 seismograms, we plot record sections normalising each waveform by its absolute maximum amplitude, excluding the *S*-waves from the plot windows. We sorted seismograms by increasing source-receiver distance and aligned by direct *P*-arrival time. Phase recognition in the selected dataset was made through visual inspection on the record sections. Record sections for the whole dataset were analysed dividing the large number of stations in angular sectors of about 45 to 60 degrees of azimuth. Figure 4 shows an example of a record section for two different azimuths (an ample choice of record sections is available in the supplementary material). We generally observe the x-phase along the direction perpendicular to the slab face (left in Figure 4) from 600 to about

1000 km from the epicentre and in the range from 330 to 30 degrees. For the complementary sector, from 30 to 300 clockwise, record sections never show the x-phase.

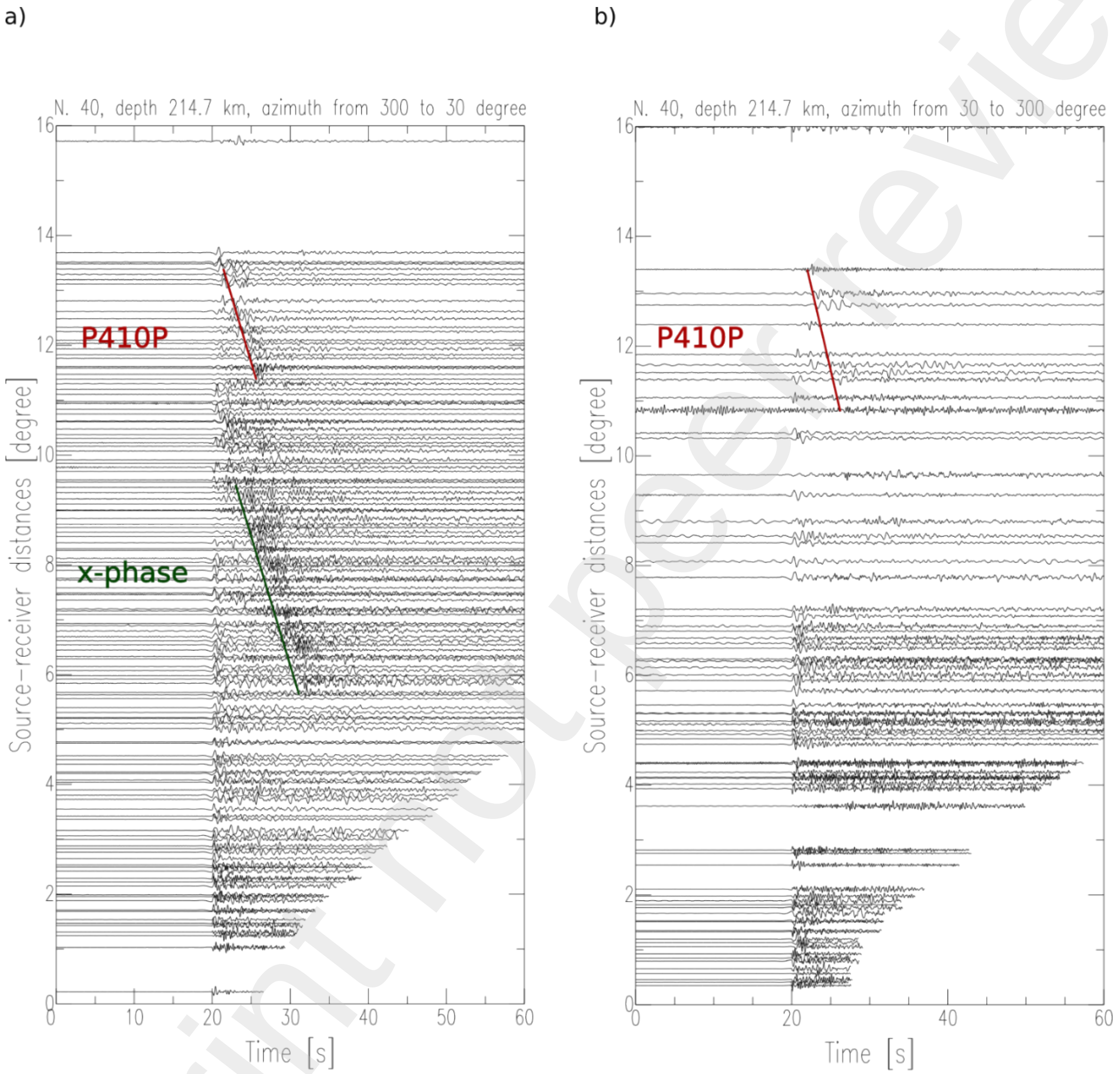

Figure 4 – (a) *Record Section in the azimuth 300-30 for an intermediate depth earthquake of the Southern Tyrrhenian Subduction Zone.* ***(b)*** *Record Section for the same earthquake but for the complementary azimuth. The x-phase is visible only in the stations to the north of the epicentre at a distance from 600 km to about 1000 km.*

The *x-phase* is rather prominent and easy to recognise. It generally appears in the vertical component as an impulsive arrival with an amplitude about two times larger than the first *P*-arrival (Figure 5a). It is also clearly visible in the horizontal component and again it has a larger amplitude with respect to the direct P wave. The x-phase has similar amplitude on the vertical and NS component, and both are about the double with respect to the EW component (Figure 5b).

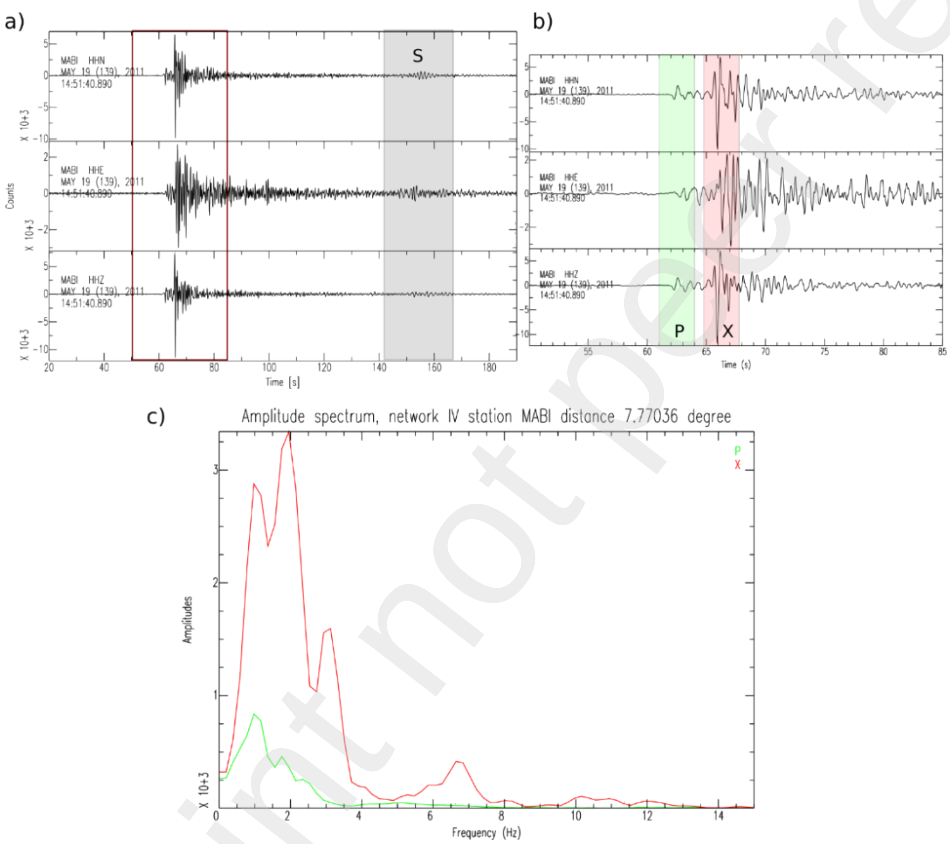

*Figure 5 - **(a)** Three component waveforms of station MABI located at 7.7 degrees from epicentre. The red box indicates the window of Figure b; **(b)** the green and the red boxes show the time window on which the amplitude spectra of the P and x-phase are computed. The arrival on the vertical and the NS component is impulsive while it is less clear in the EW component. The station*

is located to the north of the epicentre; ***(c)*** *Amplitude spectra of the direct P wave (green) and the later arrival (red).*

At greater distances, from 11 degrees onwards, we found another arrival after the direct *P*-wave that is well reproduced by the 410 km discontinuity. We also noticed that the *x-phase* has, generally, a higher frequency content in comparison to the direct P wave. We have not done systematic analyses on the frequency content as it is not the goal of this paper and it will be part of a future work. We have seen, however, that the x-phase is characterised by a frequency of about 2 Hz while the direct *P*-wave of about 1 Hz (Figure 5c).

4. Results

The diagrams in Figure 6 shows the particle motion of the first *P*-arrival and the secondary x-phase at MABI station located 8.23° away from the epicentre. The selected earthquake occurred at a depth of 298 km beneath the Aeolian Islands. The ray-path for both phases deviates of about 5° from the theoretical source-receiver back-azimuth. The *x-phase* shows a typical *P*-wave particle motion and we verified that this is a general observation for the *x-phase*. These characteristics indicate that the *x-phase* is a compressional *P*-wave that travels in a less attenuating path than the direct *P*-wave.

After analysing all the available record sections, we notice that the *x-phase* appears at about 6 degrees from the epicenter, it is not present in all the events, and it is dependent on the azimuth. The time difference between direct *P* and the secondary wave, at the distance where the phase appears, is 10 seconds, as an average. The arrival time difference between the direct *P* and the x-phase decreases with epicentral distance and, at about 9 degrees, the x-phase reaches the first onset.

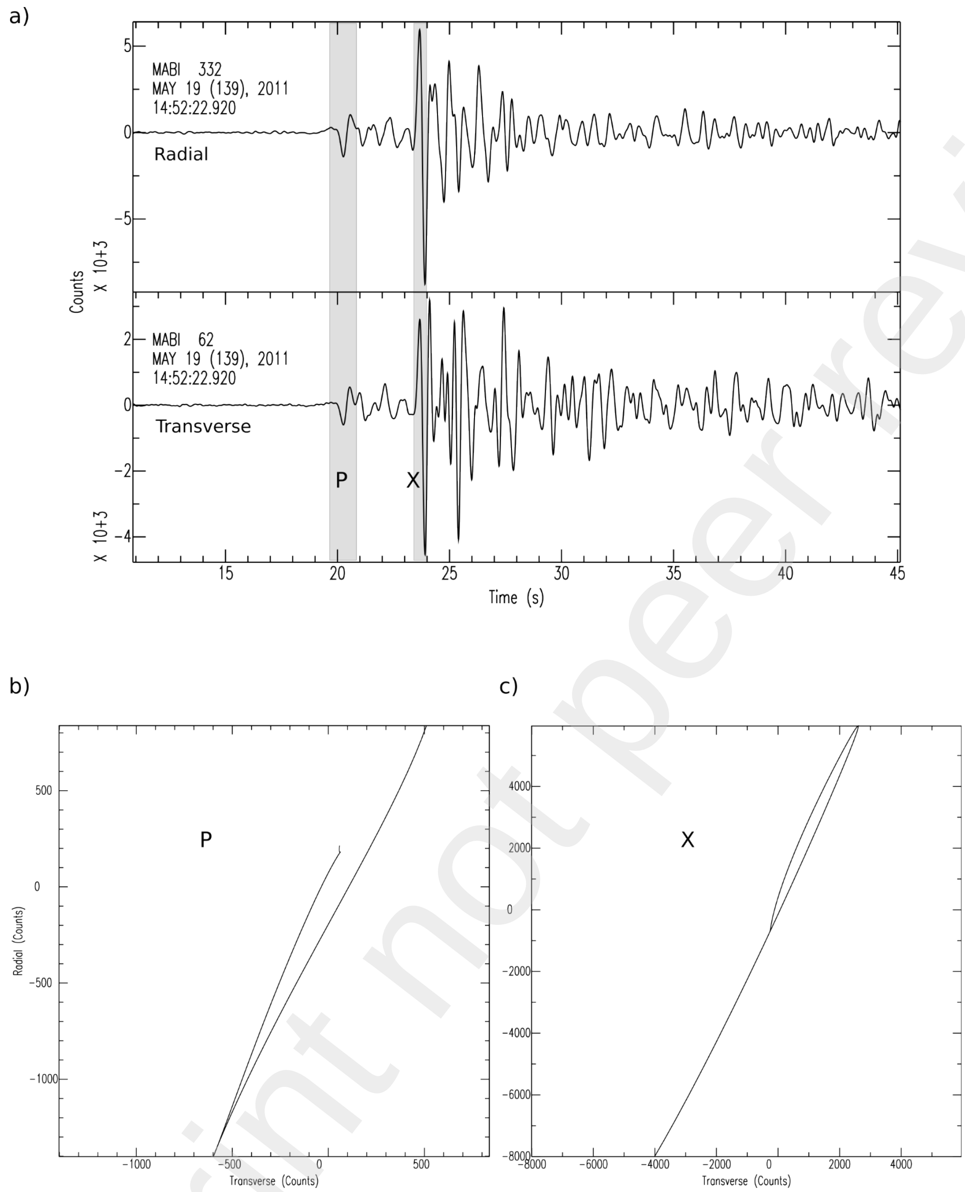

***Figure 6 - (a)** Radial and transverse waveforms of station MABI. The grey boxes highlight the time windows of which the particle motions are computed; **(b)** particle motion diagram of the direct P wave and **(c)** of the x-phase.*

The x-phase has an apparent velocity of about 11 km/s. Record sections show that the apparent velocity after 9 degrees and after the x-phase reaches the first onset is equal to the direct P wave and not to that of the *x-phase*. This means that the *x-phase* reaches the surface only between 6 and 9 degrees and not after or before these distances. This is a strong constrain in the x-phase interpretation. We then plot the seismograms in function of hypocenters for each station. The arrival time decreases with increasing depths at each station (Figure 7). This suggests that the *x-phase* is in some way related with a deeper interface, probably within the slab. The deeper the earthquake, the shorter the difference in the arrival time between the direct P wave and the x-phase.

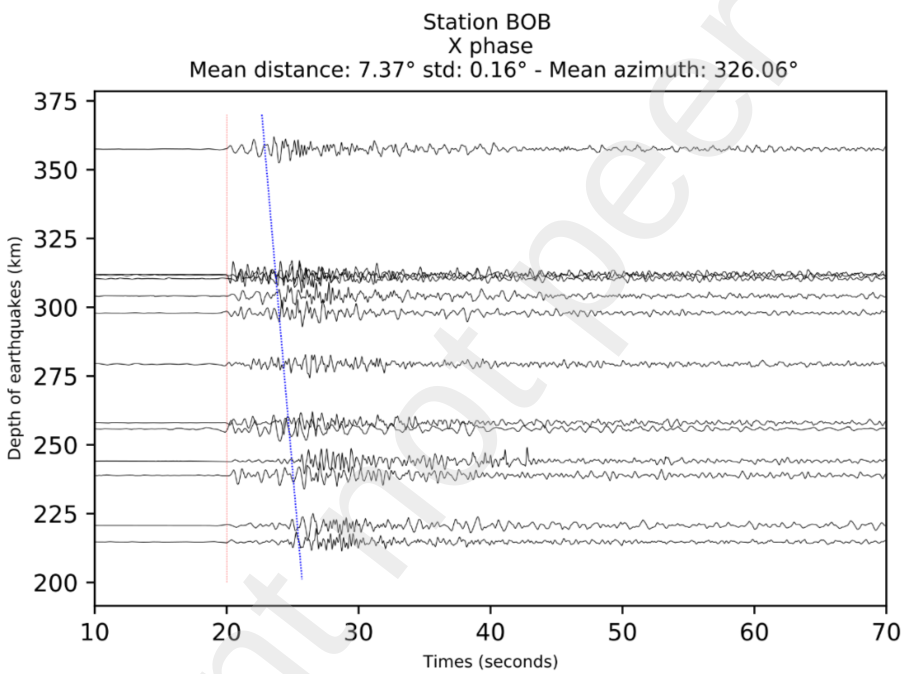

***Figure** 7 – Vertical waveforms recorded at the seismic station BOB for different earthquakes. They are sorted by earthquake depth and aligned by P first arrivals on the y-axis (the red vertical line). The blue line highlights the x-phase arrivals.*

Only seismograms of stations located in the northerly quadrants with respect to the epicentre show the later *P*-arrival, as shown in Figures 2 and 4. Results can be generalised in the following way.

All the seismograms between 6 and 9 degrees from earthquakes with hypocentre below the Aeolian Arc and in the depth range 220 to 312 km show the x-phase, a compressional P wave, as in the example of Figure 8a. Earthquakes with hypocentre in the western side of Calabria's coasts never show the secondary phase, but only the phase associated to the ~410 km discontinuity (Figure 8b). Earthquakes beneath the coast of Calabria occur at the same depth range of the earthquakes beneath the Aeolian Islands. Earthquakes with hypocentre deeper than 400 km do not show neither the secondary phase nor a phase associated to the 410 km discontinuity (Figure 8c). Figure 9 shows the spatial distribution of the three different cases. A further peculiar observation is from profile A–B of Figure 3b. It shows that the hypocentres of the earthquake where we observed the *x-phase*, below the Aeolian Islands, are concentrated in the bottom part of the seismic zone, near to the interface between the lower edges of the slab with the surrounding mantle. We compared two seismic catalogues (INGV Italian Seismological Instrumental and Parametric Database available at http://cnt.rm.ingv.it/iside and D. La Torre personal communication) and the hypocentres, although slightly different, show the same pattern.

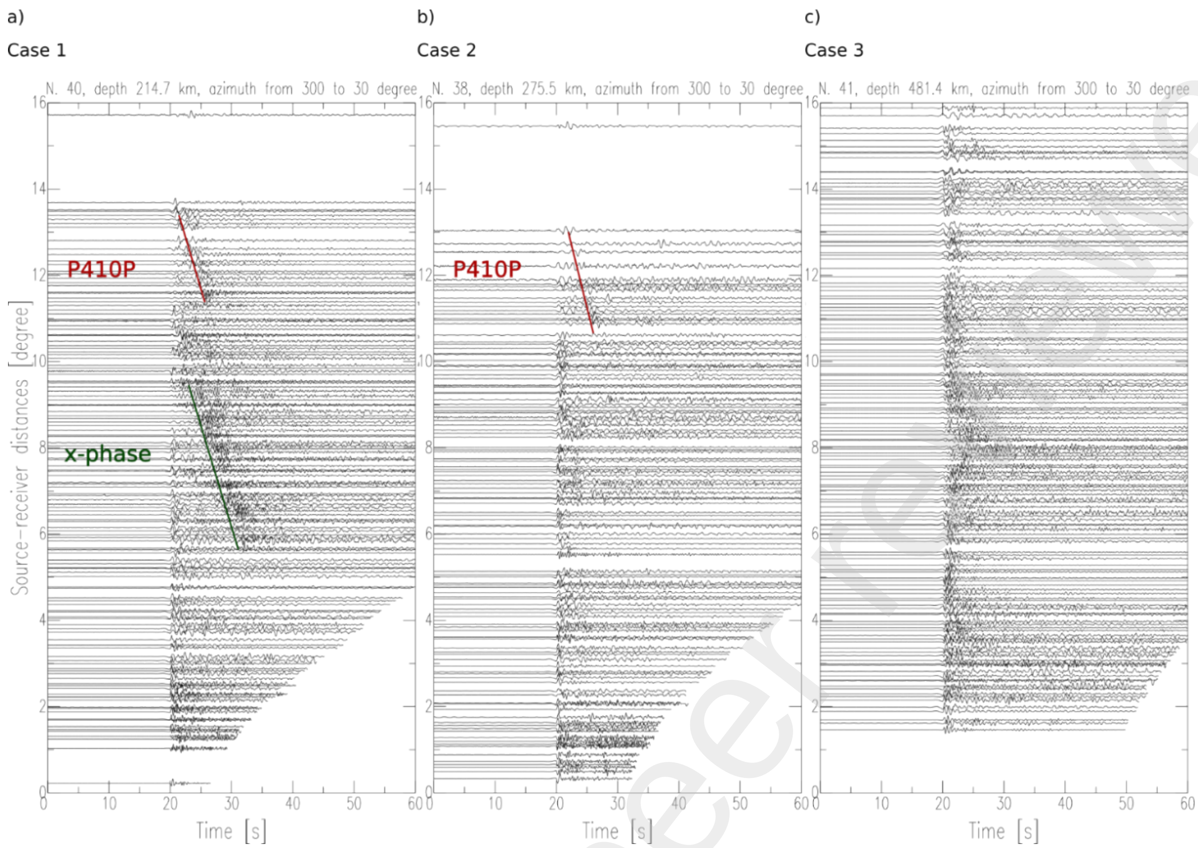

Figure 8 - *Examples of record sections of the three cases we discuss in the text. The "N." in the title corresponds to number id in the map of the Figure 8 (N. 40, 38, 41).*

The seismological constraints derived from the observations made in this work, allow us to design a simple 2D modelling by means of fitting the arrival times. The final goal is to understand the nature and origin of the x-phase. We are aware that a 2D approach is a first approximation of a complex 3D geometry as it is the Southern Tyrrhenian subduction zone and future work will include a full 3D model to take into account the complex three-dimensional geometry of the problem.

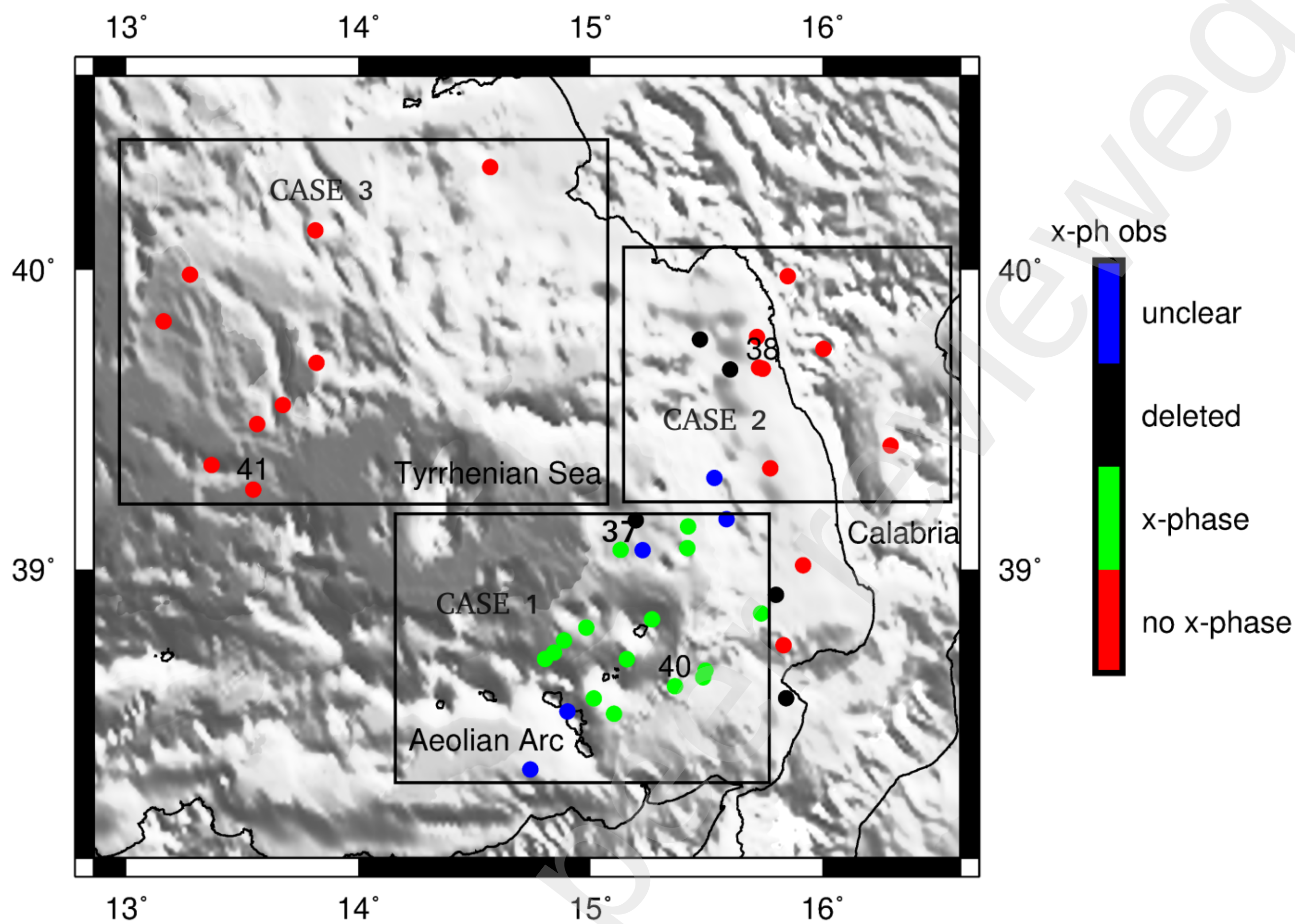

Figure 9 – Map distribution of the earthquakes that show the secondary seismic phase (green dots), that do not show the x-phase (red dots) and those earthquakes where the presence of the x-phase is unclear (blue dots).

We calculated theoretical travel time curves with Seis83 software (Červený, V., & I. Pšenčík, 1984) that makes use of ray-tracing technique (Červený et al., 1977) with the graphical interface model (Komminaho, 1998) and ZPLOT (Zelt, 1994).

Several models were tested to match the arrival times of the *x-phase*. We used IASP91 velocity model (Kennett and Engdahl, 1991) to represent the velocity structure outside the slab (Figure 10a), whereas the slab boundaries were constrained by seismicity distribution (Figure 3b).

Following Pino and Helmberger, (1997), the 410-km discontinuity is raised up to a depth of 370 km, as generally observed in subduction zones (Collier et al., 2001). According to tomographic studies (Amato et al., 1993; Scarfì et al., 2018; Spakman et al., 1993), the subducting lithosphere is characterized by positive velocity anomalies. We increased the velocity inside the slab in different run by a percentage between 1.5% and 5% to the IASP91 velocity values.

The arrivals of the direct P wave are well fitted by a subducting lithosphere with an average increment of 1.5% of IASP91 velocity model, whereas the *x-phase* requires much faster velocities, at least 3% higher than IASP91**.** Hence, we introduced a narrow high velocity layer, HVL, in the lowermost subducted lithospheric mantle, in the region where we observe the hypocentre of the earthquakes with the secondary phase with an average increase of the velocity up to 3% with respect to IASP91. Compressional velocities in the HVL between 250 and 370 km depth are from 8.9 to 9.15 km/s. The model is able to fit the arrival times of the x-phase for all the deep earthquakes below the Aeolian Island we have modelled (Figure 10c).

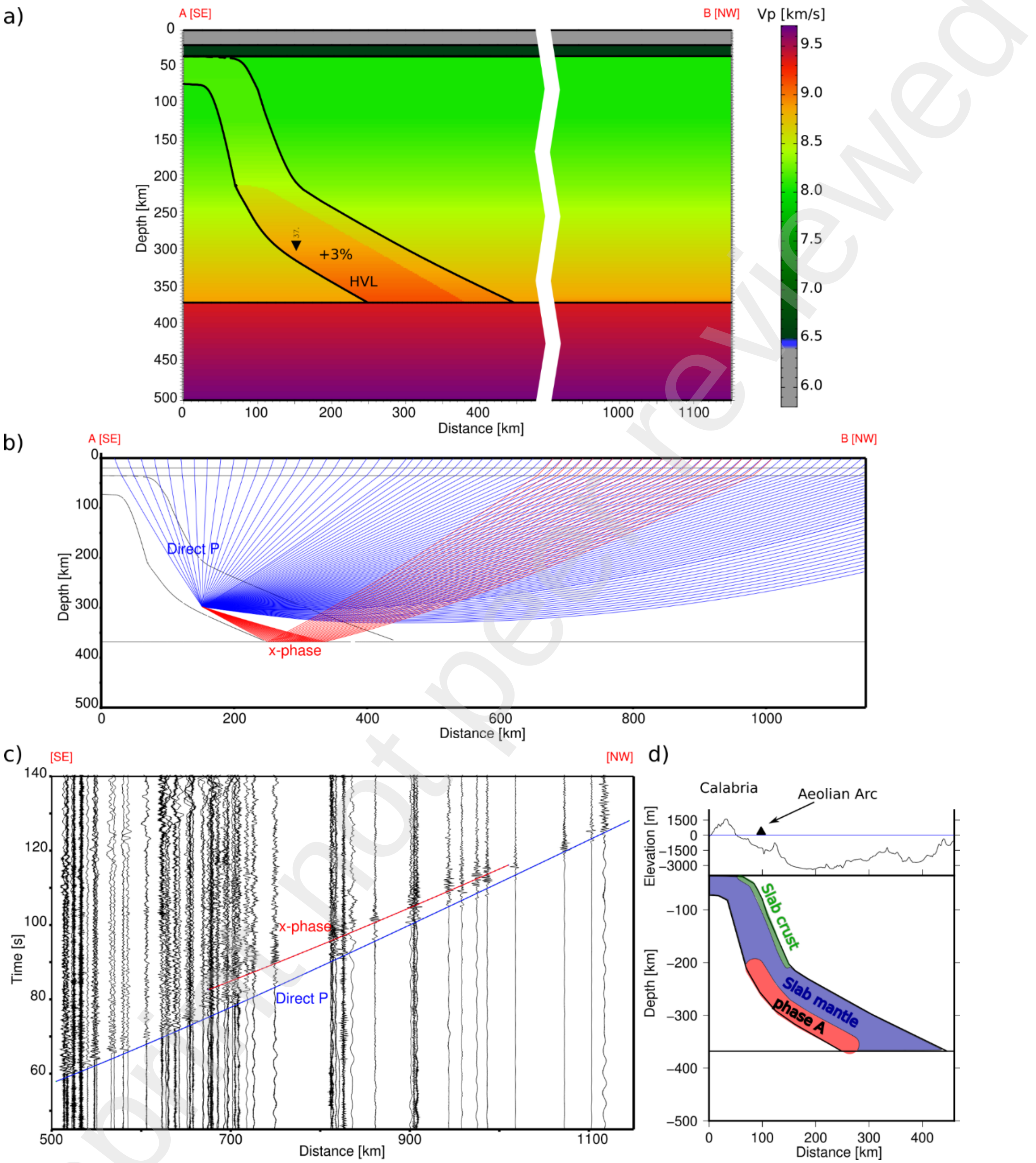

Figure 10 – (a) *2D velocity model, section trace in the Figure 2 (n.b. the section orientation is opposite of those in Figure 3b-c to have increasing distances rightwards). The black triangle is the 2011 earthquake (N. 37) with x-phase;* ***(b)*** *Calculated ray paths for the earthquake N. 37;* ***(c)***

calculated travel time curves on the observed record section of earthquake N. 37. The blue line shows the calculated direct P wave arrivals, and the red line is for the x-phase; ***(d)*** *Sketch of the possible petrology and thickness of the HVL.*

The introduction of a HVL provides the explanation to most of the positive and negative observations we have done in this work. It explains why the secondary phase is not observed in very deep earthquakes, below the 410 km discontinuity. It may explain also the different frequency content of the direct P wave if compared to that of the x-phase traveling along a different, probably less attenuating, path. It also provides an explanation why we see the *x-phase* only at specific epicentral distances (between 6 and 9 degrees).

Between the unresolved issues, the reasons why we do not observe the later arrival in the earthquakes located below the Calabrian Arc slab is the most intriguing. There are clear geometric differences between these two sectors of the slab and probably a combination of geometry of the slab and its velocity structure is a necessary condition to generate the secondary phase. This is one of the main goals of a future 3D model.

5. Discussion and Conclusions

We have described the nature and origin of a later arrival observed in intermediate-depth and deep earthquakes of the Tyrrhenian subduction zone at stations from 6 to 9 degrees from epicentres, towards north. Only earthquakes beneath the Aeolian Islands and in the depth range between 215–320 km generate this later *P*-arrival. The 2D modelling shows that a combination of velocity structure and geometric characteristics is able to reproduce rather well the positive and negative observations of the whole dataset.

Travel times indicate that the phase is not a depth phase. The main characteristic of depth phases is that the difference of time between a depth phase onset and the *P*-onset is an increasing function of the epicentral distance (Murphy & Barker, 2006). For the same reason, it is not even a *SP*-wave, which is a direct *S*-wave traveling upward and converted at the upper boundary of the slab, as analysed in Zhao et al. (1997) for the Japan slab. The later arrival described in this work is a *P*-wave that propagates downward in a high velocity layer located in the lowermost part of the subducted lithospheric mantle.

As far as we know, a HVL, as the one we have introduced in this work, has not been previously described from a seismological point of view. The dubitative question mark in our title reflects some assumptions contained in the modelling and other considerations that should be verified. These refer to three main questions. Why tomographic images available for the Tyrrhenian subduction zone do not show such a narrow HVL? Why the fast and late *P*-arrival has not been observed elsewhere, in other subduction systems? Are *P*-wave velocities as fast as 9.1 km/s reasonable at 300-350 km depth within a slab?

There are plenty of tomography results published for the Tyrrhenian subduction zone that use different datasets and inversion techniques (Amato et al., 1993; Chiarabba et al., 2008; Lucente et al., 1999; Selvaggi & Chiarabba, 1995; Spakman et al, 1993). None of them shows a clear well defined HVL, although all agree that at depths between 200 and 400 km, the *P*-velocity is higher than the velocity of the surrounding mantle but not at the level of the HVL we have introduced. An answer is that the thickness of the HVL could be as wide as 20–30 km and such layer is probably too narrow to be detected by the course grid generally used to model the mantle at those depths. The high velocities of the HVL could then be averaged within the general high *P*-velocity at those depths, masking the real velocity anomaly of the HVL.

The fact that we see the later *P*-arrival only in the Southern Tyrrhenian Subduction Zone, then, is probably due to the peculiar combination of the velocity structure, geometric conditions, as said before, as well as the station distribution in front of the slab. Concerning the Tyrrhenian subduction, we are particularly lucky as it has the whole Europe and its numerous seismological stations in front of it, spanning distances evenly for thousands of km. Such network geometry is not easy to find in other subduction zones. All the subductions along the Pacific have a less favourable network geometry. The distance between 6 and 9 degrees from the epicentre for most of the pacific subductions are either in the sea or in less monitored areas. That is probably why the *x-phase* is not a common finding from other subduction zones, although it is not excluded that it could be observed elsewhere. We also checked seismograms from Hellenic subduction and from some Vrancea intermediate-depth earthquakes without any interesting result. We noticed, anyway, that in Greece and in Romania there are no *x-phase*. Systematic research all around subduction zones will be part of the extension of this research in the future.

Finally, a comparison with laboratory experiments on mineral transformations conducted at upper mantle conditions, provides a nice, elegant and simple explanation for the nature of our observations and allows us to make some important inferences on the origin of the *x-phase*.
We have shown that the earthquakes with the *x-phase* are located in the uppermost mantle lithosphere of the subducted slab, near the lower boundary of the seismic plate, between 215 to about 320 km of depth. The representing lithology that composes the lithospheric mantle at these depths is generally lherzolite and harzburgite (e.g., Hacker et al., 2003a). These rocks commonly

enter into the subduction as locally hydrated, with water incorporated into OH-bearing minerals like antigorite serpentine and chlorite (see Figure 5 in Hacker et al., 2003a). The slab deepening during subduction causes devolatilization reactions (e.g., Hacker et al., 2003a, b) facilitating the embrittlement of these minerals. This process gives rise to earthquakes. When antigorite serpentine and chlorite react out at depth, not all the water escapes from the system and some can be still hold into a meta-stable mineral phase in the upper-mantle deep slab (e.g., Sclar et al., 1965; Cai et al., 2021). This mineral phase, which is a dense magnesium hydrated silicate, has been called in literature *phase A* (Sclar et al., 1965). Phase A is stable at higher pressure and temperature conditions and its importance is because carries water deep into the Earth (Wunder & Schreyer, 1992; Fumagalli et al., 2001). Recent ultrasonic measurements of compressional waves on *phase A* in a cold subduction show an increase of P-velocities to the level introduced in the HVL model (Cai et al., 2021) and at depths from about 200 km and down. In addition, these depths are consistent with the range where we model the HVL in the Tyrrhenian subduction. Therefore, we interpret the HVL as related to the presence of the dense hydrous magnesium silicate *phase A*, formed after antigorite breakdown as inferred from laboratory experiments and predicted by phase equilibria in cold subduction zones (van Keken et al., 2011; Cai et al., 2021), as the Tyrrhenian subduction seems to be. This is the first direct seismological observation of the phase A in the subduction process.

Data availability

For the creation of this manuscript the data were extracted from the following archives. Earthquakes data are from the Italian Seismological Instrumental and Parametric Data-base (ISIDE

Working Group, 2007). Waveforms are extracted from the European Integrated Data Archive (EIDA, http://eida.ingv.it/) infrastructure within the Observatories & Research Facilities for European Seismology (ORFEUS) and Federation of Digital Seismograph Networks (FDSN) and from the Incorporated Research Institutions for Seismology Data Management Centre. (IRIS DMC, https://ds.iris.edu/ds/nodes/dmc/data/types/waveform-data/). Most of the data are from the networks having the identifiers: IV, MN, NI, SI, SL, CH, GU, OE (INGV Seismological Data Centre, 2006; MedNet Project Partner Institutions, 1990; OGS and University of Trieste, 2002; Slovenian Environment Agency, 1990; Swiss Seismological Service at ETH Zurich, 1983; University of Genoa, 1967; ZAMG - Zentralanstalt für Meterologie und Geodynamik, 1987).

Acknowledgments

This work has been funded by INGV internal funding (Bando Ricerca Libera 2019) and supported by a subsidy from the Polish Ministry of Education and Science for the Institute of Geophysics, Polish Academy of Sciences.

Figures were made using the SAC software (Goldstein et al., 2003; Goldstein and Snoke, 2005) the Generic Mapping Tools (GMT), version 5 (Wessel et al., 2013) available at https://www.genericmapping-tools.org and the Obspy tool (Beyreuther et al., 2010).

We thank Prof. Johannes Schweitzer for its insightful comments and advice in the first stage of the work.

References

Abers, G. A. (2000). Hydrated subducted crust at 100–250 km depth. Earth and Planetary Science Letters, 176(3-4), 323-330. https://doi.org/10.1016/S0012-821X(00)00007-8

Abers, G. A. (2005). Seismic low-velocity layer at the top of subducting slabs: observations, predictions, and systematics. Physics of the Earth and Planetary Interiors, 149(1-2), 7-29. https://doi.org/10.1016/j.pepi.2004.10.002

Amato, A., Alessandrini, B., Cimini, G., Frepoli, A., & Selvaggi, G. (1993). Active and remnant subducted slabs beneath Italy: evidence from seismic tomography and seismicity. Annals of Geophysics, 36(2). https://doi.org/10.4401/ag-4272

Anderson, H., & J. Jackson (1987), Active tectonics of the Adriatic region, Geophys. J. R. Astron. Soc., 91, 937 – 983.

Beyreuther, M., Barsch, R., Krischer, L., Megies, T., Behr, Y., Wassermann J., (2010) ObsPy: A Python Toolbox for Seismology SRL, 81(3), 530-533. 10.1785/gssrl.81.3.530

Cai, N., Qi, X., Chen, T., Wang, S., Yu, T., Wang, Y., et al. (2021). Enhanced Visibility of Subduction Slabs by the Formation of Dense Hydrous Phase A. Geophysical Research Letters, 48(19), 1–10. https://doi.org/10.1029/2021GL095487.

Červený, V., Molotkov, I. A., & Pšenčík, I. (1977). Ray method in seismology. Univerzita Karlova, https://doi.org/10.1016/S0065-2687(06)48001-8

Červený, V. & Pšenčík, I., (1984). SEIS83 - Numerical modelling of seismic wave fields in 2-D laterally varying layered structures by the ray method, in Documentation of Earthquake

Algorithms, Rep. SE-35, pp. 36–40, ed. Engdal, World Data Center (A) for Solid Earth Geophysics.

Chiarabba, C., De Gori, P., & Speranza, F. (2008). The southern Tyrrhenian subduction zone: deep geometry, magmatism and Plio-Pleistocene evolution. Earth and Planetary Science Letters, 268(3-4), 408-423., https://doi.org/10.1016/j.epsl.2008.01.036

Cimini, G. B., & Marchetti, A. (2006). Deep structure of peninsular Italy from seismic tomography and subcrustal seismicity. Annals of Geophysics. http://hdl.handle.net/2122/2000

Collier, J. D., Helffrich, G. R., & Wood, B. J. (2001). Seismic discontinuities and subduction zones. Physics of the Earth and Planetary Interiors, 127(1-4), 35-49. https://doi.org/10.1016/S0031-9201(01)00220-5

D'Agostino, N., E. D'Anastasio, A. Gervasi, I. Guerra, M. R. Nedimović, L. Seeber, and M. Steckler (2011), Forearc extension and slow rollback of the Calabrian Arc from GPS measurements, Geophys. Res. Lett., 38, L17304, doi:10.1029/2011GL048270.

Essen, K., Braatz, M., Ceranna, L., Friederich, W., & Meier, T. (2009). Numerical modelling of seismic wave propagation along the plate contact of the Hellenic Subduction Zone-the influence of a deep subduction channel. Geophysical Journal International, 179(3), 1737-1756, https://doi.org/10.1111/j.1365-246X.2009.04369.x

Faccenna, C., Becker, T.W., Lucente, F.P., Jolivet, L., & Rossetti F., (2001) History of subduction and back-arc extension in the Central Mediterranean, Geophysical Journal International, 145, 809-820, https://doi.org/10.1046/j.0956-540x.2001.01435.x

Frepoli, A., Selvaggi, G., Chiarabba, C., & Amato, A. (1996). State of stress in the Southern Tyrrhenian subduction zone from fault-plane solutions. Geophysical Journal International, 125(3), 879-891. https://doi.org/10.1111/j.1365-246X.1996.tb06031.x

Fukao, Y., Kanjo, K. & Nakamura, I. (1978), Deep seismic zone as an upper mantle reflector of body waves. Nature 272, 606–608. https://doi.org/10.1038/272606a0

Fumagalli, P., Stixrude, L., Poli, S., & Snyder, D. (2001). The 10Å phase: A high-pressure expandable sheet silicate stable during subduction of hydrated lithosphere. Earth and Planetary Science Letters, 186(2), 125–141. https://doi.org/10.1016/S0012-821X(01)002382

Goldstein, P., D. Dodge, M. Firpo, Lee Minner (2003) "SAC2000: Signal processing and analysis tools for seismologists and engineers, invited contribution to "The IASPEI International Handbook of Earthquake and Engineering Seismology", Edited by WHK Lee, H. Kanamori, P.C. Jennings, and C. Kisslinger, Academic Press, London.

Goldstein, P. A. U. L., & Snoke, A. (2005). SAC availability for the IRIS community. Incorporated Research Institutions for Seismology Newsletter, 7(UCRL-JRNL-211140).

Hacker, B. R., Abers, G. A., & Peacock, S. M. (2003a). Subduction factory 1. Theoretical mineralogy, densities, seismic wave speeds, and H_2O contents. Journal of Geophysical Research: Solid Earth, 108(B1), 1–26. https://doi.org/10.1029/2001jb001127

Hacker, B. R., Peacock, S. M., Abers, G. A., & Holloway, S. D. (2003b). Subduction factory 2. Are intermediate-depth earthquakes in subducting slabs linked to metamorphic dehydration reactions? Journal of Geophysical Research: Solid Earth, 108(B1). https://doi.org/10.1029/2001jb001129

Hasegawa, A., Umino, N., & Takagi, A. (1978). Double-planed structure of the deep seismic zone in the northeastern Japan arc. Tectonophysics, 47(1-2), 43-58.

Hori, S. (1990). Seismic waves guided by untransformed oceanic crust subducting into the mantle: the case of the Kanto district, central Japan. Tectonophysics, 176(3-4), 355-376.

INGV Seismological Data Centre, (2006). *Rete Sismica Nazionale (RSN)*. Istituto Nazionale di Geofisica e Vulcanologia (INGV), Italy. https://doi.org/10.13127/SD/X0FXNH7QFY

ISIDe Working Group. (2007). Italian Seismological Instrumental and Parametric Database (ISIDe). Istituto Nazionale di Geofisica e Vulcanologia (INGV). https://doi.org/10.13127/ISIDE

Kennett, B.L.N. and Engdahl, E.R. (1991), Traveltimes for global earthquake location and phase identification. Geophysical Journal International, 105: 429-465. https://doi.org/10.1111/j.1365-246X.1991.tb06724.x

Komminaho, K., (1998). Software Manual for Programs MODEL and XRAYS: A Graphical interface for SEIS83 Program Package, University of Oulu, Dep. of Geophys., Rep. 20, 31 pp.

Lucente, F. P., Chiarabba, C., Cimini, G. B., & Giardini, D. (1999). Tomographic constraints on the geodynamic evolution of the Italian region. Journal of Geophysical Research: Solid Earth, 104 (B9), 20307-20327. https://doi.org/10.1029/1999JB900147

Martin, S., Rietbrock, A., Haberland, C. & Asch, G., 2003. Guided waves propagating in subducted oceanic crust, J. geophys. Res., 108 (B11), 2536, https://doi.org/10.1029/2003JB002450 .

Martin, S. & Rietbrock, A., 2006. Guided waves at subduction zones: dependencies on slab geometry, receiver locations and earthquake sources, Geophys. J. Int., 167, 693–704, https://doi.org/10.1111/j.1365-246X.2006.02963.x

Matsuzawa, T., Umino, N., Hasegawa, A., & Takagi, A. (1986). Upper mantle velocity structure estimated from PS-converted wave beneath the north-eastern Japan Arc. Geophysical Journal International, 86(3), 767-787, https://doi.org/10.1111/j.1365-246X.1986.tb00659.x

MedNet Project Partner Institutions. (1990, January 1). Mediterranean Very Broadband Seismographic Network (MedNet). Istituto Nazionale di Geofisica e Vulcanologia (INGV). https://doi.org/10.13127/SD/FBBBTDTD6Q

Murphy, J. R., & Barker, B. W. (2006). Improved focal-depth determination through automated identification of the seismic depth phases pP and sP. Bulletin of the Seismological Society of America, 96(4A), 1213-1229, https://doi.org/10.1785/0120050259

Obara, K., & Sato, H. (1988). Existence of an S wave reflector near the upper plane of the double seismic zone beneath the Southern Kanto District, Japan, J. Geophys. Res., 93(B12), 15037–15045, https://doi.org/10.1029/JB093iB12p15037.

OGS (Istituto Nazionale di Oceanografia e di Geofisica Sperimentale) and University of Trieste (2002): North-East Italy Broadband Network. International Federation of Digital Seismograph Networks. Dataset/Seismic Network. https://doi.org/10.7914/SN/NI

Ohmi, S., & Hori, S. (2000). Seismic wave conversion near the upper boundary of the Pacific plate beneath the Kanto district, Japan. Geophysical Journal International, 141(1), 136-148, https://doi.org/10.1046/j.1365-246X.2000.00086.x

Pino, N. A. and D. V. Helmberger (1997), Upper mantle compressional velocity structure beneath the West Mediterranean Basin, J. Geophys. Res., 102(B2), 2953–2967, https://doi.org/10.1029/96JB03461

Ritsema A.R. (1972) Deep earthquakes of the Tyrrhenian Sea, Geol. Mijnb., 51, 541 -545.

Scarfì, L., Barberi, G., Barreca, G., Cannavò, F., Koulakov, I., & Patanè, D. (2018). Slab narrowing in the Central Mediterranean: the Calabro-Ionian subduction zone as imaged by high resolution seismic tomography. Scientific reports, 8(1), 1-12, https://doi.org/10.1038/s41598.018-23543-8

Sclar, C. B. (1965). High-pressure synthesis and stability of a new hydrogen-bearing layer silicate in the system MgO-SiO_2-H_2O. Am. Geophys. Union Trans., 46, 184.

Selvaggi, G. (2001). Strain pattern of the Southern Tyrrhenian slab from moment tensors of deep earthquakes: implications on the down-dip velocity. Annals of Geophysics, 44(1). https://doi.org/10.4401/ag-3613

Selvaggi, G., & Chiarabba, C. (1995). Seismicity and P-wave velocity image of the Southern Tyrrhenian subduction zone. Geophysical Journal International, 121(3), 818-826. https://doi.org/10.1111/j.1365-246X.1995.tb06441.x

Slovenian Environment Agency (1990): Seismic Network of the Republic of Slovenia. International Federation of Digital Seismograph Networks. Dataset/Seismic Network. https://doi.org/10.7914/SN/SL

Spakman, W., van der Lee, S., & van der Hilst, R. (1993). Travel-time tomography of the European-Mediterranean mantle down to 1400 km. Physics of the Earth and Planetary Interiors, 79(1-2), 3-74. https://doi.org/10.1016/0031-9201(93)90142-V

Sun, D., Miller, M. S., Agostinetti, N. P., Asimow, P. D., & Li, D. (2014). High frequency seismic waves and slab structures beneath Italy. Earth and Planetary Science Letters, 391, 212-223, https://doi.org/10.1016/j.epsl.2014.01.034.

Swiss Seismological Service (SED) at ETH Zurich; (1983): National Seismic Networks of Switzerland; ETH Zürich. Other/Seismic Network. https://doi.org/10.12686/sed/networks/ch

University of Genoa (1967): Regional Seismic Network of North Western Italy. International Federation of Digital Seismograph Networks. Dataset/Seismic Network. https://doi.org/10.7914/SN/GU

van Keken, P. E., B. R. Hacker, E. M. Syracuse, and G. A. Abers (2011), Subduction factory: 4. Depth-dependent flux of H2O from subducting slabs worldwide, J. Geophys. Res., 116, B01401, doi:10.1029/2010JB007922.

Wessel, P., Smith, W. H., Scharroo, R., Luis, J., & Wobbe, F. (2013). Generic mapping tools: improved version released. Eos, Transactions American Geophysical Union, 94(45), 409-410. https://doi.org/10.1002/2013EO45000.

Wunder, B., & Schreyer, W. (1992). Metastability of the 10-Å phase in the system MgO-SiO2-H2O (MSH). what about hydrous MSH phases in subduction zones? Journal of Petrology, 33(4), 877–889. https://doi.org/10.1093/petrology/33.4.877

ZAMG - Zentralanstalt für Meterologie und Geodynamik (1987): Austrian Seismic Network. International Federation of Digital Seismograph Networks. Dataset/Seismic Network. https://doi.org/10.7914/SN/OE

Zelt, C.A., 1994. Software Package ZPLOT, Bullard Laboratories, University of Cambridge.

Zhao, D., Matsuzawa, T., & Hasegawa, A. (1997). Morphology of the subducting slab boundary in the northeastern Japan arc. Physics of the Earth and Planetary Interiors,102(1-2), 89-104. https://doi.org/10.1016/S0031-9201(96)03258-X

Zhao, C.A., (2019). Importance of later phases in seismic tomography. Physics of the Earth and Planetary Interiors, 296, 106314, https://doi.org/10.1016/j.pepi.2019.106314.